

Size-Dependent Reactivity of Diamond Nanoparticles

Oliver A. Williams,^{†,*} Jakob Hees,[†] Christel Dieker,[‡] Wolfgang Jäger,[‡] Lutz Kirste,[†] and Christoph E. Nebel[†]

[†]Fraunhofer Institute for Solid State Physics, Tullastrasse 72, Freiburg 79108, Germany, and [‡]Institut of Materials Science, Christian-Albrechts-Universität zu Kiel, Kaiserstrasse 2, Kiel 24143, Germany

ABSTRACT Photonic active diamond nanoparticles attract increasing attention from a wide community for applications in drug delivery and monitoring experiments as they do not bleach or blink over extended periods of time. To be utilized, the size of these diamond nanoparticles needs to be around 4 nm. Cluster formation is therefore the major problem. In this paper we introduce a new technique to modify the surface of particles with hydrogen, which prevents cluster formation in buffer solution and which is a perfect starting condition for chemical surface modifications. By annealing aggregated nanodiamond powder in hydrogen gas, the large (>100 nm) aggregates are broken down into their core (~ 4 nm) particles. Dispersion of these particles into water *via* high power ultrasound and high speed centrifugation, results in a monodisperse nanodiamond colloid, with exceptional long time stability in a wide range of pH, and with high positive zeta potential (>60 mV). The large change in zeta potential resulting from this gas treatment demonstrates that nanodiamond particle surfaces are able to react with molecular hydrogen at relatively low temperatures, a phenomenon not witnessed with larger (20 nm) diamond particles or bulk diamond surfaces.

KEYWORDS: nanoparticle · nanodiamond · zeta potential · drug delivery · nanomedicine

Since the discovery of nanodiamond particles in detonation soot,¹ and their subsequent mass production, a diverse array of applications have been proposed ranging from drug delivery² to seeds for the growth of diamond thin films.³ A major weakness in the currently available material is the presence of large tightly bound aggregates which are formed during the cooling cycle of the detonation shock wave.⁴ These aggregates cannot be broken up by high power ultrasound alone, and the reduction of them into the primary core particles has been an active research area for over 20 years. Several novel methods have been demonstrated to produce single-digit-size nanodiamond particles, but all have drawbacks specific to the process applied. For example, bead milling results in particles contaminated with zirconia,⁴ the complete removal of which is almost impossible. Graphitization/oxidation⁵ or burning in air⁶ results in a significant loss of raw material and operates within a very narrow

temperature window. All of these approaches rely on techniques to disintegrate the strong sp^2 -bonded matrix that binds the core sp^3 particles together, which explains why purely wet chemical approaches such as adding surfactants are not successful in realizing monodisperse colloids.⁷

The realization of nanodiamond particle applications is heavily dependent on the cost-effective production of clean, long-term, stable monodispersed particles with defined surface chemistry. In this work, hydrogenation of detonation nanodiamond powders is shown to be possible *via* annealing in hydrogen gas. This effect is based on the reaction of the sp^2 shells and bonding matrix between particles with hydrogen gas. Thus, the effect is restricted to particle sizes smaller than 10 nm which exhibit reconstructed surfaces and significant sp^2 bonding due to high surface to volume fractions. The hydrogenation process results in a breakdown of these large aggregates of diamond bonded in an sp^2 matrix into primary particles with defined surface functional groups. The resulting colloids have very high positive zeta potential over a wide range of pH and a narrow distribution of particle sizes centering on the core particle size. The colloidal solution is stable in the long term, showing no cluster formation over extended periods of time which is an important requirement for bioapplications like in drug delivery and biolabeling techniques.²

RESULTS

Diamond particles produced *via* detonation synthesis were treated as detailed in the Methods section. Colloids from the resulting particles were then characterized by

*Address correspondence to oliver.williams@iaf.fraunhofer.de.

Received for review April 12, 2010 and accepted July 6, 2010.

Published online July 12, 2010.
10.1021/nn100748k

© 2010 American Chemical Society

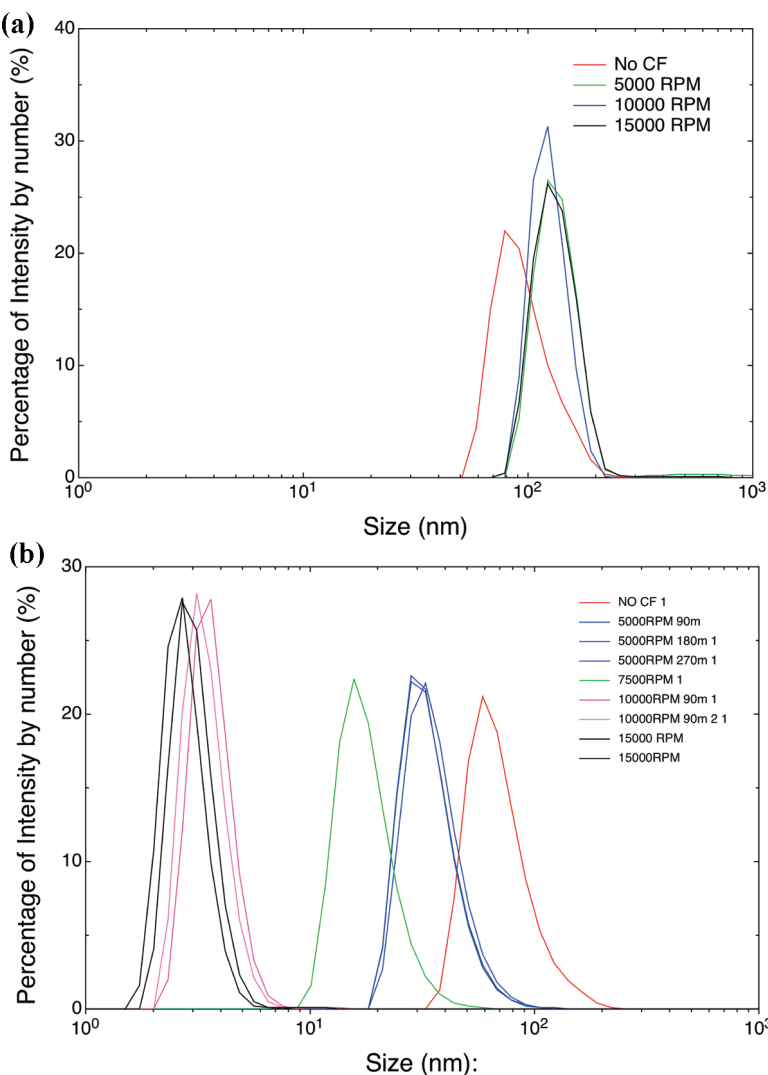


Figure 1. (a) DLS size distribution after various centrifugations of untreated powder, (b) DLS size distribution after various centrifugations of hydrogenated powder.

dynamic light scattering (DLS), X-ray diffraction (XRD), transmission electron microscopy (TEM), and Fourier transform infrared (FTIR) microscopy (see Methods section) as detailed below. The resulting particle sizes of the nanodiamond colloids are plotted in Figure 1. In Figure 1a the particle size distribution of the untreated powder before and after numerous centrifugations is shown. It can be seen that almost independently of centrifugation, the dominant particle size is over 100 nm, with no evidence of any smaller particles. The particle size distribution of the colloid made with the treated powder is shown in Figure 1b. It can be seen that even before centrifugation, the particle size distribution is now centered on 58 nm. Particles are significantly smaller than those of the untreated powder. After centrifugation, the peak of the particle size distribution shifts to lower sizes. After centrifugation at 5000 rpm it reduces to 28–32 nm, after 75000 rpm to 16 nm, and then to 2–4 nm after centrifugation above 10000 rpm. The core particle size is reached after >10000 rpm centrifugation for 90 min, and the colloid can be defined

as fundamentally monodisperse. Further centrifugation at higher speeds (15000 rpm) results in only a small reduction in the median and standard deviation of the particle size distribution. The final yield is approximately 50%.

Figure 2 shows the zeta potential as a function of pH as determined by dynamic light scattering of the aqueous colloids made from the untreated and hydrogenated nanodiamond powders. It can be seen from this plot that the treatment of the powder has a significant effect on the zeta potential. The untreated powder has a negative zeta potential over the entire pH range which becomes progressively more negative as the pH is increased, which is common for acid cleaned commercial nanodiamond powders.⁴ There was evidence of an isoelectric point in the untreated powder at pH values around 2 or below but these measurements also resulted in corrosion of the electrodes so they are omitted in case of error. After annealing in hydrogen gas the zeta potential becomes positive for all pH values. The pH is constant around +40 mV from pH

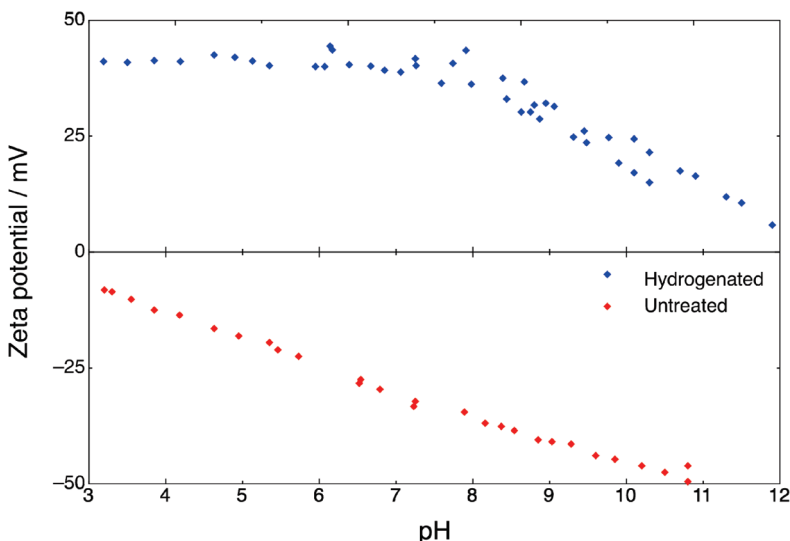


Figure 2. Zeta potential of untreated and hydrogenated nanodiamond powder as a function of pH.

3 until pH 7 where it decreases with increasing pH. At higher pH values the hydrogenated sample showed a very low zeta potential which was difficult to measure and again resulted in electrode degradation. Neither solutions show a clear iso-electric point within this pH range, although the directions of the curves suggest they may exist at extreme pH values. It should be noted that the solution of hydrogenated diamond particles showed a zeta potential as high as +70 mV when measured immediately after preparation. The reduced zeta potential in the titration series is most likely due to very mild contamination from the autotitrator and to prolonged exposure to air.

Figure 3 shows photographs of the above solutions before and after centrifugation, the solution having been left to stand for one hour. In Figure 3A it can be seen that the untreated powder is not stable in solution, as expected from the low zeta potential recorded in Figure 2.

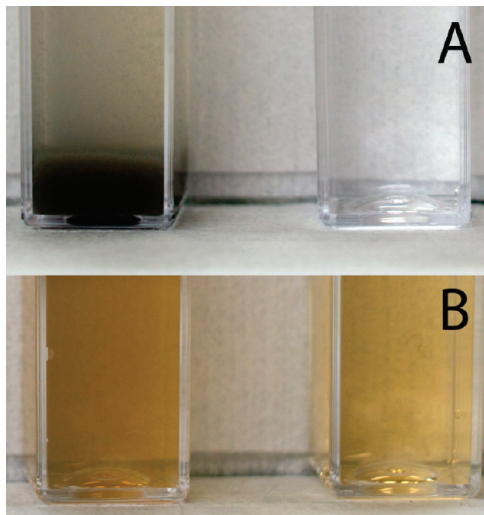


Figure 3. Photographs of (A) untreated powder and (B) treated powder in solution before (left) and after (right) centrifugation at 15000 rpm.

Figure 2. The left of the image shows the powder after 1 h in the solution. The mixture is already collapsing, forming aggregates, with the bulk of the material already settled on the bottom of the cuvette. A gradient of lighter solution with increasing height is detected. Centrifugation exacerbates the situation and after doing so it can be seen that the powder is almost completely removed from the solution as shown on the right of Figure 3A. The remaining concentration of powder in this solution is thus very low. However, there is a strong difference in Figure 3B; the left image shows that the treated powder is fundamentally stable. Some larger particles are eventually removed from the solution and it has a slightly opaque quality as compared to the right of the image. Here, after centrifugation the solution appears diaphanous and is completely stable over long durations.

To characterize the crystalline quality of the particles, X-ray diffraction measurements were performed. 0/20 X-ray diffraction data of the two powders are shown in Figure 4. The diffraction pattern of nanodiamond displays three peaks at $2\theta = 43.8$ (111), 75.2 (220), and 91.1 (311) corresponding to the cubic planes of diamond. There is a noticeable peak broadening due to the small crystal size of the nanodiamond crystals and associated stress and defects. There is no obvious background from amorphous carbon indicating the high quality of the nanodiamond before and after treatment. The diffraction data for before and after treatment are identical, indicating that there is no change in crystallite size or quality, meaning that no graphitization arises from this process.

The results from X-ray diffraction are confirmed by TEM investigations of the two different powders as shown in Figure 5. These investigations confirm that the individual diamond particles possess crystalline core regions. In Figure 5a the particles of the untreated powder are very tightly aggregated into sizes of 100

nm and greater. Individual diamond particles as observed for the treated powder (Figure 5c), though slightly aggregated due to the TEM specimen preparation) were not observed. After hydrogenation the particle aggregates are broken up into much smaller sizes as shown in Figure 5c. It should be noted that the small particles have aggregated slightly on drying for TEM specimen preparation due to the surface tension of water. These aggregates are, however, much smaller, and they clearly do show the single particles (typical sizes between 4 and 8 nm). Also single particles are observed. It is obvious from inspecting a number of similarly prepared TEM specimens that the density of the particle aggregates is significantly reduced. Evident in high-resolution TEM images of both treated and untreated particles are onion like shells surrounding the particle cores as seen in Figure 5b,d. These are well-known to occur at the surfaces of detonation nanodiamond particles,^{8,9} and a more detailed description of these shells can be found elsewhere.¹⁰

FTIR spectroscopy has been used to define the surface functional groups of both powders. FTIR spectra of both untreated and hydrogenated material are shown in Figure 6. The differences between the two spectra are pronounced. Starting with the low wave numbers, the broad band starting from 1000 cm^{-1} with maxima at 1140 cm^{-1} is due to the superposition of bands associated with nitrogen and the ethereal $\equiv\text{C}-\text{O}-\text{C}\equiv$ group.¹¹ This is significantly reduced after hydrogen treatment. The hydrogenated sample shows no maxima at the ethereal peak position. The spectral region below 1500 cm^{-1} contains absorption bands of $\text{C}-\text{C}$, $\text{C}-\text{O}$, and $\text{C}-\text{N}$ as well as deformation $\text{O}-\text{H}$ and $\text{C}-\text{H}$ vibrations and is thus highly convoluted.¹² A detailed description of all the possible contributing features is beyond the scope of this work; however, of particular note is the peak at 1332 cm^{-1} which is assigned to the $\text{C}-\text{C}$ stretching vibrations of the diamond lattice with nitrogenous impurities.¹³ It is significantly more pronounced in the spectra of the hydrogenated material due to the reduced convolution with the aforementioned $\text{C}-\text{O}$ and $\text{O}-\text{H}$ states. Evidence of $\text{C}-\text{N}$ stretching vibrations is apparent in both samples at 1250 cm^{-1} ,¹⁴ with an attenuated intensity in the hydrogenated spectrum. The peak at 1384 cm^{-1} is due to the OH bending vibration in COOH ¹⁵ and is only present in the untreated material. Another small peak of note in the hydrogenated spectra is at 1465 cm^{-1} , related to bending modes of CH , CH_2 , and CH_3 .¹⁶ The bulk of the differences in the two spectra occur in the region between 1500 and 3000 cm^{-1} . The features between 1600 and 1700 cm^{-1} are mostly related to water and OH bending and thus are not used for comparison here, a more detailed explanation is available elsewhere.¹⁷ However, it should be noted the 1620 cm^{-1} band is associated with an OH bending mode and is not present in the hydrogenated sample.¹⁷ By far the most

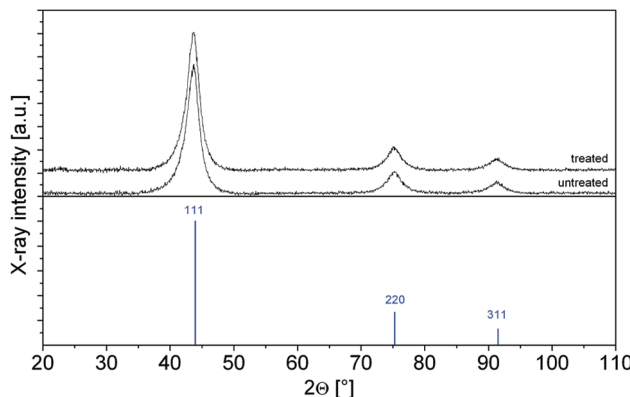


Figure 4. $0/2\theta$ X-ray diffraction data of untreated and treated powders.

significant change in the two spectra is in a band with a peak at 1772 cm^{-1} which is intense in the untreated material but absent in the hydrogenated material. This is unambiguous evidence of $\text{C}=\text{O}$ stretching modes and thus of carbonyl groups on the untreated powder surface.¹³ The next most significant change is in the appearance of bands at 2875 – 2920 cm^{-1} in the spectra of the hydrogenated material. These bands are due to stretching modes of CH_2 and CH_3 .¹³

DISCUSSION

Clearly, in order to explain the vast difference in zeta potentials of the treated and untreated powders shown in Figure 2, there must be a significant difference in the surface charge of the diamond particles. It is not a sufficient explanation that the aggregated particles have just been broken down thermally as the zeta potential is not a function of particle size. Thisulti-

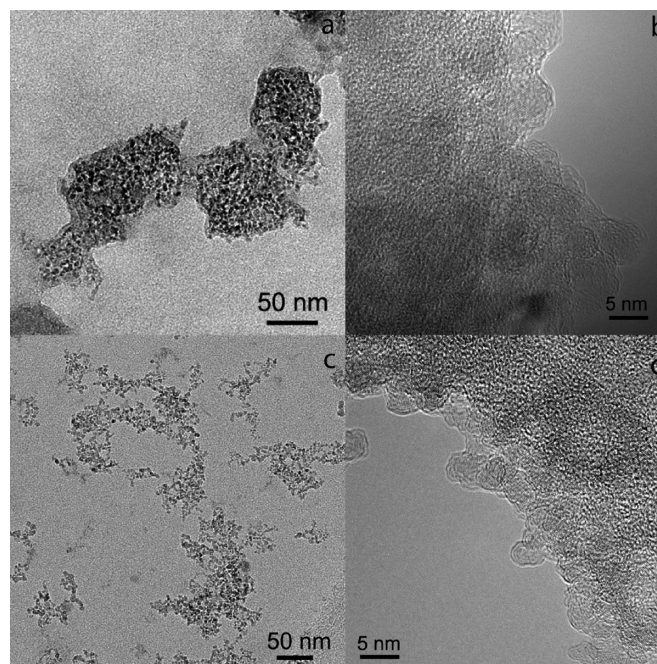


Figure 5. Bright-field transmission electron micrographs of (a) untreated powder, (c) treated powder. High-resolution transmission electron micrographs of (b) untreated powder, (d) treated powder.

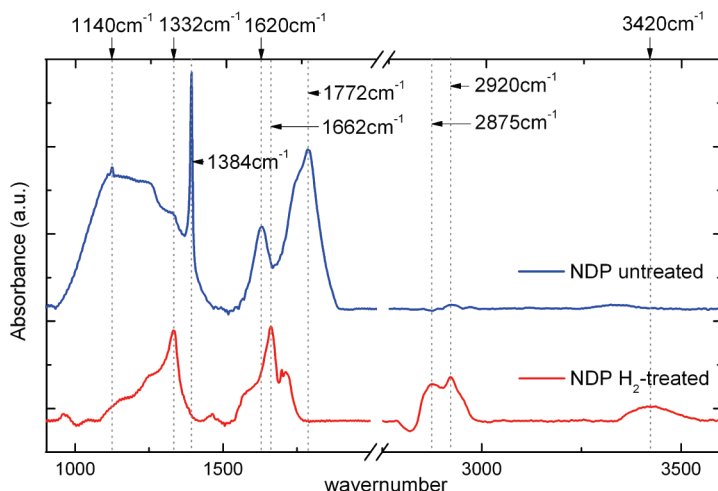


Figure 6. FTIR spectra of treated and untreated powders.

mately means that there must be a significant change of functional groups on the diamond nanoparticle surface to shift their net charge over 80 mV to the positive. The resulting zeta potential of +70 mV is among the highest reported in the literature.¹⁸ The untreated particles have a negative zeta potential which is commonly found in commercial nanodiamond powders due to acid cleaning steps leaving oxygen groups on the surface, such as carboxyl, lactones, etc.¹⁹

The FTIR measurements of Figure 6 clearly confirm the presence of these oxygen groups as well as several others. The dissociation of these acid groups (particularly carboxyl groups) can result in a negative zeta potential. Obviously, as one reduces pH this negative potential is compensated by protons⁺ due to the acidity of the solution, thus the magnitude of the negative zeta potential decreases, that is, becomes more positive. As pH is increased it becomes progressively more negative due to the OH⁻ groups of the solution. Thus the pH dependence of the zeta potential of the untreated powder can be entirely explained by the presence of oxygen groups and their interaction with the protons and hydroxide ions in the solution. It should be noted that for biological applications it is desirable for the particles to have a large zeta potential at acidic pH values common *in vivo* rather than at alkali pH. Thus, the region of stability (zeta potential greater than 30, or less than -30 mV) is inappropriate for such applications with the untreated powder.

The relatively low zeta potential of -10 mV explains the instability of the colloid as shown in Figure 3A. The TEM image in Figure 5a also confirms the presence of the large aggregates seen in the DLS Figure 1a. Thus, the untreated material possesses all the common properties of commercially available material which have been published in detail elsewhere.²⁰ Clearly, from Figure 4 there is no appreciable damage to the core diamond particles resulting from the hydrogen annealing. It is possible and rather likely that weakly bonded reactive carbon is removed from the

particles by hydrogenation,²¹ but this is not visible by XRD in such small quantities.

The DLS data of Figure 1b and the TEM image of Figure 5c show that after hydrogenation the nanodiamond particles of the detonation diamond are left behind and are no longer bound as large aggregates. Figure 6 confirms that the surfaces of detonation nanodiamond particles are able to react with hydrogen gas at temperatures as low as 500 °C. The concentration of oxygen containing surface groups such as $\equiv\text{C}-\text{O}-\text{C}\equiv$, $\text{C}=\text{O}$, $\text{O}-\text{H}$, etc. (features at 1000–1140, 1772 and 1384, and 1620 cm^{-1} , respectively) are significantly reduced, leaving behind hydrogen containing groups such as CH , CH_2 , and CH_3 (features at 1465 and 2875–2920 cm^{-1}). Oxygen is clearly replaced by hydrogen, surprisingly at low temperatures and with a molecular source, that is, pure H_2 gas. This is rather unusual as hydrogen gas must be dissociated by very high temperatures (>2200 °C) such as with a hot filament or *via* microwave plasma in order to terminate diamond surfaces.²² Thus, there has to be a new effect arising from nanosized particles which allows such a reaction to occur. For example heating bulk diamond at 500 °C will show no hydrogen termination of the surface. In active carbon and carbon black it is well-known that essentially all oxygen containing groups can be driven from the surface by hydrogen annealing.²¹ This is mostly explained by the driving off of oxygen containing functional groups from the edges of carbon crystallites, where most of the functional groups exist. We assign the effect therefore to the high surface to volume fraction driving the phenomena. It is a size dependent effect. Attempts to treat larger (20 nm) diamond particles *via* the same approach were unsuccessful. Transmission electron microscopy clearly shows that the sp^2 onion like shells are still present after hydrogen treatment (Figure 5d). These are exactly the kind of structures one sees in carbon black materials.²³

A second unusual result of the hydrogen gas treatment is the generation of a positive zeta potential. In

carbon black materials, this is commonly explained by the removal of the strong acidic groups by hydrogen, leaving basic groups at the edges of carbon layers.²⁴ These basic groups can be dissociated to generate a net positive charge on the core particle. However, it is most common that the density of these basic groups is significantly lower than the previous acidic groups, so it seems unlikely they would be able to render such a large zeta potential.²⁴ The FTIR spectrum of the treated powder in Figure 6 also shows little evidence of these groups although their presence could be to some extent masked by a water layer on the particle surfaces. Protonation of conventional oxygen functional groups is rather unlikely to occur in simple aqueous solutions as used here, especially as considering positive zeta potentials are observed even under relatively mild acidity.²⁵

Another explanation of carbon basicity is oxygen free Lewis base sites on the basal planes,²¹ that is, within the graphene layers of carbons. Pyrone-type groups have been invoked to explain a mild carbon basicity when there is a significant concentration of oxygen on the surface,²⁶ but this is not the case here and the effect is more than mild.

The closest explanation for carbon basicity from the vast literature of carbon black and activated carbon literature is probably that of the electron–donor–acceptor (EDA) complex.²⁶ In this complex electrons from π or π^* states can interact with oxonium ions (H_3O^+), which are formed in acidic water. Transmission electron microscopy clearly confirms that there is a significant fraction of π bonding in these nanoparticles due to the onion-like shells (Figure 5d). Thus they could provide π states for this interaction. It has been predicted that a finite amount of sp^2 bonding on diamond nanoparticles below a certain size is inevitable.²⁷ The amount of noncrystalline carbon has been shown to be up to 10% by neutron diffraction;²⁸ hence, one cannot consider the chemistry of detonation nanodiamond particles without considering the significant concentration of sp^2 bonding at particle surfaces. The EDA complex could also explain positive zeta potentials in nanodiamonds that have been mechanically milled and have had no contact with hydrogen,¹⁸ due to their sig-

nificant surface sp^2 content. This complex could also explain why it is difficult to make such monodisperse colloids in other solvents, that is, because of the lack of oxonium ions.

Figure 2 contains strong evidence for this in that the zeta potential is constant under pH 7. Thus, when the water is slightly acidic, there are enough oxonium ions to bind to the relatively low concentration of diamond particles in the solution. This means that decreasing the pH and therefore increasing the proton concentration and oxonium ion concentration will have little effect on the zeta potential as a small shift to acidity from neutral has already provided sufficient oxonium ions for electron out diffusion. There are no more electrons available for out diffusion so adding oxonium ions has no effect. However, as one goes toward alkali pH from neutral there is a strong reduction in the zeta potential due to a reduction in the availability of oxonium ions and compensation of the positive charge due to an increasing concentration of negative OH ions. The hydrogenated powder shows high positive zeta potential over all acidic pH values, and thus is stable for *in vivo* applications such as drug delivery and biomarking where the majority of the body is in the acidic pH range.

CONCLUSIONS

A facile and new method to purify and disperse nanodiamond powder at its core particle size has been demonstrated. The result is highly stable monodisperse nanodiamond colloids with particle sizes 3–4 nm and zeta potential greater than +60 mV. This approach relies on the fact that nanodiamond particles will react with molecular hydrogen gas at relatively low temperatures. The positive zeta potential has been explained by electron out diffusion into oxonium ions which are present in water and humid air. This phenomenon is very similar to the EDA complex in carbon black and other disordered carbons. The effect only works on detonation nanodiamond particles, as larger particles have a significantly lower sp^2 surface coverage and the sp^3 regions do not react with molecular hydrogen gas at these temperatures.

METHODS

Commercially available nanodiamond powders (G01 grade) were sourced from Plasmachem GmbH. For the gas treatment, 0.4 g of powder was placed in a vacuum oven and evacuated to a base pressure better than $1 = 10^{-6}$ mbar. Hydrogen gas, purified to 99.99999% by a palladium membrane was flowed through the chamber at 50 sccm, and the pressure was maintained at 10 mbar. The powder was resistively heated to 500 °C as determined by a single wavelength optical pyrometer. After 5 h of exposure, the sample was cooled to room temperature under hydrogen gas flow, evacuated to high vacuum, and vented. Aqueous colloids were made from both treated and untreated powder by immersing 0.1 g of powder in 200 mL of deionized water and dispersing with a high-power ultrasonic horn (Sonics Vibra-cell VCX 500). The condi-

tions were 250 W at a duty cycle of 3:2 (on/off) for 5 h under aggressive liquid cooling. The temperature of the solution was maintained below 20 °C. The solutions were allowed to settle for 24 h and then decanted to remove any large mass contaminants such as the unavoidable titanium alloy from the sonotrode. Solutions were then centrifuged for 90 min at various speeds from 5000 to 15000 rpm in a Universal 320R centrifuge.

DLS particle size and zeta potential measurements were made with a Malvern Zetasizer Nano ZS equipped with a 633 nm laser. Measurements were made in the back scattering configuration (173°). Particle size distributions are the average of 100 30 s scans and zeta potential of 300 scans. The bulk refractive index of bulk diamond (2.4) was used to convert the measured intensity/size distributions in number of particles/size distribu-

tions. This was necessary as all nanodiamond colloids are very slightly polydisperse, with less than 0.1% of the particles around 10 times larger than the dominant core particle. As the Rayleigh approximation predicts the intensity of the light scattered to be proportional to diameter,⁶ the small concentration of larger particles would dominate the intensity spectrum. It was found that very little error is generated by deviations from the refractive index which is expected for Rayleigh scattering. The Rayleigh approximation is reasonable as the particle size is <10% of the laser wavelength, < 1% in the smallest cases. The error in the measurement is estimated at below 2%. Zeta potential measurements made with the Malvern Zetasizer Nano ZS were calibrated with an aqueous suspension of polymer microspheres at pH 9.2, which in turn was referenced by the standard NIST1980. pH titrations were made with the Malvern autotitrator option. HCl was used as the acid titrant and NaOH for the base. Both concentrations were 0.1 M.

XRD measurements (0/2θ scans) were recorded in reflection geometry with a focusing powder diffractometer equipped with a Cu sealed tube and a bended Ge 111 monochromator providing CuK α_1 radiation. The measurements were performed in the 2θ ranges of 20–110° with a step width of 0.05°. For the microscopic investigations by TEM, bright-field and high-resolution TEM imaging of particle and aggregates were performed in a TECNAI F30 at 300 kV. The TEM specimens were prepared by dispersing the particle suspensions with and without ultrasonification onto TEM holey carbon–copper grids and by subsequent drying in air. Optimized high-resolution imaging conditions were chosen in order to reduce delocalization effects on the particle image contrast and to ensure unambiguous interpretability, especially also in view of the presence and sizes of the onion-like shells surrounding the particle cores. Presently, further experiments are in preparation that apply the methods of aberration-corrected TEM for a quantitative evaluation of the nanoparticle contrast.

FTIR spectra were recorded using a Bruker Equinox 55 spectrometer with a DTGS detector at a resolution of 2 cm⁻¹ and 64 scans. The sample chamber was purged with pure nitrogen gas. Samples were prepared as KBr pellets containing 2 mg diamond nanopowder ground thoroughly with 140 mg KBr powder and pressed in a 7 mm die using an ICL KBr Quick Press. All samples and the control sample containing solely KBr powder were pretreated under the same conditions. To measure IR spectra with reduced interference from adsorbed water, sample pellets were dried in a vacuum oven at 150 °C for 12 h and directly transferred into the sample chamber of the spectrometer.

Acknowledgment. This work was supported by the Fraunhofer Attract award “Hybrid HF-MEMS Filters for GHz-Communication and capillary MEMS systems for chemical and bio-chemical Sensing—COMBIO”.

REFERENCES AND NOTES

1. Danilenko, V. V. On the History of the Discovery of Nanodiamond Synthesis. *Phys. Solid State* **2004**, *46*, 595–599.
2. Chen, M.; Pierstorff, E. D.; Lam, R.; Li, S. Y.; Huang, H.; Osawa, E.; Ho, D. Nanodiamond-Mediated Delivery of Water-Insoluble Therapeutics. *ACS Nano* **2009**, *3*, 2016–2022.
3. Williams, O. A.; Douheret, O.; Daenen, M.; Haenen, K.; Osawa, E.; Takahashi, M. Enhanced Diamond Nucleation on Monodispersed Nanocrystalline Diamond. *Chem. Phys. Lett.* **2007**, *445*, 255–258.
4. Kruger, A.; Kataoka, F.; Ozawa, M.; Fujino, T.; Suzuki, Y.; Aleksenskii, A. E.; Vul', A. Y.; Osawa, E. Unusually Tight Aggregation in Detonation Nanodiamond: Identification and Disintegration. *CARBON* **2005**, *43*, 1722–1730.
5. Xu, K.; Xue, Q. J. A New Method for Deaggregation of Nanodiamond from Explosive Detonation: Graphitization–Oxidation Method. *Phys. Solid State* **2004**, *46*, 649–650.
6. Osswald, S.; Yushin, G.; Mochalin, V.; Kucheyev, S. O.; Gogotsi, Y. Control of sp²/sp³ Carbon Ratio and Surface Chemistry of Nanodiamond Powders by Selective Oxidation in Air. *J. Am. Chem. Soc.* **2006**, *128*, 11635–11642.
7. Xu, Y. Y.; Yu, Z. M.; Zhu, Y. M.; Wang, B. C. Effect of Sodium Oleate Adsorption on the Colloidal Stability and Zeta Potential of Detonation Synthesized Diamond Particles in Aqueous Solutions. *Diamond Relat. Mater.* **2005**, *14*, 206–212.
8. Barnard, A. S.; Russo, S. P.; Snook, I. K. Coexistence of Bucky Diamond with Nanodiamond and Fullerene Carbon Phases. *Phys. Rev. B* **2003**, *68*, 073406.
9. Kuznetsov, V. L.; Zilberman, I. L.; Butenko, Y. V.; Chuvalin, A. L.; Segall, B. Theoretical Study of the Formation of Closed Curved Graphite-like Structures During Annealing of Diamond Surface. *J. Appl. Phys.* **1999**, *86*, 863–870.
10. Shenderova, O. A.; Zhirnov, V. V.; Brenner, D. W. Carbon Nanostructures. *Crit. Rev. Solid State Mater. Sci.* **2002**, *27*, 227–356.
11. Kulakova, I. I. Surface Chemistry of Nanodiamonds. *Phys. Solid State* **2004**, *46*, 636–643.
12. Mironov, E.; Koretz, A.; Petrov, E. Detonation Synthesis Ultradispersed Diamond Structural Properties Investigation by Infrared Absorption. *Diamond Relat. Mater.* **2002**, *11*, 872–876.
13. Jiang, T. L.; Xu, K.; Ji, S. F. FTIR Studies on the Spectral Changes of the Surface Functional Groups of Ultradispersed Diamond Powder Synthesized by Explosive Detonation after Treatment in Hydrogen, Nitrogen, Methane and Air at Different Temperatures. *J. Chem. Soc., Faraday Trans.* **1996**, *92*, 3401–3406.
14. Misra, A.; Tyagi, P. K.; Singh, M. K.; Misra, D. S. FTIR Studies of Nitrogen Doped Carbon Nanotubes. *Diamond Relat. Mater.* **2006**, *15*, 385–388.
15. Kathi, J.; Rhee, K. Surface Modification of Multiwalled Carbon Nanotubes Using 3-Aminopropyltriethoxysilane. *J. Mater. Sci.* **2008**, *43*, 33–37.
16. Jiang, T.; Xu, K. FTIR Study of Ultradispersed Diamond Powder Synthesized by Explosive Detonation. *Carbon* **1995**, *33*, 1663–1671.
17. Ji, S. F.; Jiang, T. L.; Xu, K.; Li, S. B. FTIR Study of the Adsorption of Water on Ultradispersed Diamond Powder Surface. *Appl. Surf. Sci.* **1998**, *133*, 231–238.
18. Ozawa, M.; Inaguma, M.; Takahashi, M.; Kataoka, F.; Kruger, A.; Osawa, E. Preparation and Behavior of Brownish, Clear Nanodiamond Colloids. *Adv. Mater.* **2007**, *19*, 1201.
19. Boehm, H. P. Surface Oxides on Carbon and Their Analysis: A Critical Assessment. *Carbon* **2002**, *40*, 145–149.
20. Vul, A. Y.; Olga, A. S.; Dieter, M. G. Characterization and Physical Properties of UNCD Particles. *Ultrananocrystalline Diamond*; William Andrew Publishing: Norwich, NY, 2006; pp 379–404.
21. Menendez, J. A.; Phillips, J.; Xia, B.; Radovic, L. R. On the Modification and Characterization of Chemical Surface Properties of Activated Carbon: In the Search of Carbons with Stable Basic Properties. *Langmuir* **1996**, *12*, 4404–4410.
22. Williams, O. A.; Jackman, R. B. Surface Conductivity on Hydrogen Terminated Diamond. *Semicond. Sci. Technol.* **2003**, *18*, S34–S40.
23. *Carbon Black Science and Technology*. Marcel Dekker, Inc: New York, 1993.
24. Boehm, H. P. Some Aspects of the Surface-Chemistry of Carbon-Black and other Carbons. *Carbon* **1994**, *32*, 759–769.
25. Walker, P. L. *Chemistry and Physics of Carbon*; M. Dekker: New York, 1965; Vol. 6, p 191.
26. Leon, C.; Solar, J. M.; Calemma, V.; Radovic, L. R. Evidence for the Protonation of Basal-Plane Sites on Carbon. *Carbon* **1992**, *30*, 797–811.
27. Barnard, A. S.; Sternberg, M. Crystallinity and Surface Electrostatics of Diamond Nanocrystals. *J. Mater. Chem.* **2007**, *17*, 4811–4819.
28. Palosz, B.; Pantea, C.; Grzanka, E.; Stelmakh, S.; Proffen, T.; Zerda, T. W.; Palosz, W. Investigation of Relaxation of Nanodiamond Surface in Real and Reciprocal Spaces. *Diamond Relat. Mater.* **2006**, *15*, 1813–1817.